

UNIVERSITAT POLITÈCNICA DE CATALUNYA

Màster:

AUTOMÀTICA I ROBÒTICA

Tesi de Màster

MODELING AND SIMULATION OF A SERIES HYBRID
ELECTRIC VEHICLE PROPULSION SYSTEM

Raúl Santiago Muñoz Aguilar

Directors: Enric Fossas Colet
Arnau Dòria Cerezo

Curs Acadèmic 2009/10
Gener 2010

TECHNICAL UNIVERSITY OF CATALONIA

Master Program:

AUTOMATIC CONTROL AND ROBOTICS

Master Thesis

MODELING AND SIMULATION OF A SERIES HYBRID
ELECTRIC VEHICLE PROPULSION SYSTEM

Raúl Santiago Muñoz Aguilar

Advisers: Enric Fossas Colet
Arnau Dòria Cerezo

Academic Course 2009/10

January of 2010

A Mónica

Acknowledgments

Un agradecimiento es poco para expresar todo lo que diferentes personas han hecho para que este trabajo llegara a su culmen.

En primer lugar quiero dar gracias a Dios por su amor, luz y guía durante mi vida. A mis padres y mi familia por su formación y apoyo. A mi esposa por su amor y compañía, por esperar con paciencia durante mi formación y estar a mi lado en cada instante.

Mis directores de Tesis, Enric Fossas Colet y Arnau Dòria Cerezo, que han sacado lo mejor de mí, me han apoyado y corregido en todo momento. Han sido guías y luces en el camino, además de ser ejemplo a seguir de cara a mi futuro como investigador.

Al profesor Paul F. Puleston de la Universidad Nacional de la Plata, Argentina, con sus consejos nos dió ideas para proponer y analizar el nuevo sistema de propulsión.

A todos las personas que no haya nombrado y de alguna forma colaboraron en mi vida y en este trabajo, son tantas que necesitaría demasiadas páginas para escribirlo. Aunque no estén aquí, están en mi corazón.

Finalmente quiero agradecer a la Universidad Politénica de Cataluña, y en ésta al Instituto de Organización y Control de Sistemas Industriales y al Departamento de Ingeniería Eléctrica. A los grupos de investigación ACES (Advanced Control of Energy Systems) y REES (Renewable Electrical Energy Systems).

Abstract

Two problems related with hybrid electric vehicles have been analyzed in this dissertation. The first one consists in proposing a propulsion system scheme for the vehicle and the second one consist in modeling it.

In order to set a propulsion system scheme, the standard configurations for the hybrid electric vehicles are presented as well as some variations of the series topologies. Then, a novel configuration which is composed by a synchronous machine and an induction machine is also presented.

As said before, the second problem consist in modeling this novel configuration. The reduced model of each machine of the dynamical model is described using the dq -transformation. Bond Graph and Port-Controlled Hamiltonian approaches are also used to describe the WRSM, the DFIM and the whole system models.

Finally, the analysis of the power flowing through the system and the regenerative braking possibilities are done.

Contents

Acknowledgments	VII
Abstract	IX
Contents	XII
List of Figures	XIII
Acronyms	XIV
Glossary of symbols	XV
1 Introduction	1
1.1 Motivation	1
1.2 Thesis Objectives	3
1.3 Main contributions of the Thesis	3
1.4 Thesis organization	4
2 Hybrid Electric Vehicles	5
2.1 HEV Configurations	5
2.2 Alternative SHEV's configurations	7
2.3 Direct Synchronous-Asynchronous Conversion System	9
3 DiSAC System Model	11
3.1 Three-phase dynamical model	11
3.1.1 Wound rotor synchronous machine	12
3.1.2 Doubly-fed induction machine	14
3.2 The dq -transformation	16
3.3 The $\alpha\beta$ model	17

3.3.1	Wound rotor synchronous machine	17
3.3.2	Doubly-fed induction machine	18
3.4	The dq model	18
3.4.1	Wound rotor synchronous machine	19
3.4.2	Doubly-fed induction machine	20
3.5	System interconnection	20
4	Energy-Based Models	21
4.1	Bond Graph model	21
4.2	Port controlled Hamiltonian model	26
4.2.1	PCHS of a doubly-fed induction machine	29
4.2.2	PCHS of a wound-rotor synchronous machine	30
4.2.3	PCHS of the DiSAC system	31
4.3	Simulation results	33
5	Power Analysis for the DiSAC System	37
5.1	Power analysis of a wound-rotor synchronous machine	37
5.2	Power analysis of a doubly-fed induction machine	39
5.3	Power analysis applied to the DiSAC system	40
5.3.1	Vehicle stopped	40
5.3.2	Vehicle running at the synchronous speed	41
5.3.3	Vehicle running at twice the synchronous speed	41
5.3.4	General analysis	41
6	Conclusions and future work	43
	Bibliography	47

List of Figures

2.1	HEV topologies.	6
2.2	The joint system scheme	8
2.3	VVVF scheme	9
2.4	VVVF modified scheme	9
2.5	Electrical scheme of the DiSAC scheme.	10
3.1	Three-phase synchronous machine scheme	12
3.2	Three-phase induction machine scheme.	14
4.1	Bond Graph	22
4.2	Bond Graph model of a doubly-fed induction machine.	25
4.3	Bond Graph model of a wound-rotor synchronous machine.	26
4.4	Bond Graph model of the DiSAC system.	27
4.5	Bond Graph of the T matrix of dq -transformation	28
4.6	Bond Graph of the K matrix of dq -transformation	28
4.7	WRSM and DFIM mechanical and electrical power	34
4.8	DFIM mechanical speed and its reference.	34
4.9	Rotor, stator amplitude and field voltage	35
6.1	Electrical scheme of the modified DiSAC system.	44

Acronyms

AC: Alternating Current.
BG: Bond Graph.
CHEV: Complex Hybrid Electric Vehicle.
DC: Direct Current.
DFIM: Doubly-Fed Induction Machine.
DiSAC: Direct Synchronous-Asynchronous Conversion.
EV: Electric Vehicle.
HEV: Hybrid Electric Vehicle.
ICE: Internal Combustion Engine.
IM: (Squirrel Cage) Induction Machine.
JS: Joint System.
PCHS: Port Controlled Hamiltonian System.
PHEV: Parallel Hybrid Electric Vehicle.
PMSM: Permanent Magnet Synchronous Machine.
SHEV: Series Hybrid Electric Vehicle.
SPHEV: Series-Parallel Hybrid Electric Vehicle.
VVVF: Variable Voltage Variable Frequency System.
WRSM: Wound Rotor Synchronous Machine

Glossary of symbols

- B : mechanical damping.
 $e(t)$: effort.
 $f(t)$: flow.
 $g(x)$: interconnection matrix.
 F : amplitude of the sinusoidal waves.
 $H(x)$: Hamiltonian function.
 $\mathcal{I}_s, \mathcal{I}_r$: amplitude of the stator and rotor currents, respectively.
 i_s, i_r, i_F : stator, rotor and field current, respectively.
 i : current.
 I_n : $n \times n$ identity matrix.
 J : inertia of the rotating parts.
 $\mathcal{J}(x)$: interconnection matrix.
 $\mathcal{L}(\theta)$: inductances matrix.
 L : inductance.
 $\mathcal{L}_s, \mathcal{L}_m$ and \mathcal{L}_F : stator, magnetization and field inductances, respectively.
 L_s, L_r, L_{sr}, L_m : stator, rotor and magnetization inductances, respectively.
 n_p : number of pole pairs.
 $O_{* \times *}$: zero matrix.
 P : active power.
 Q : reactive power.
 q : generalized displacement.
 p : momentum.
 R_s, R_r, R_F : stator, rotor and field resistances, respectively.
 R : resistance.
 $\mathcal{R}(x)$: dissipation matrix.
 u, y : port variables.
 $\mathcal{V}_s, \mathcal{V}_r$: amplitude of the stator and rotor voltages, respectively.

v_s, v_r, v_F : stator, rotor and field voltage, respectively.
 v : voltage.
 x : energy variables.
 δ_s : Stator selected rotating reference.
 δ : arbitrary function of time
 λ : flux.
 $\lambda_s, \lambda_r, \lambda_F$: stator, rotor and field flux.
 Λ_s, Λ_r : amplitude of the stator and rotor fluxes, respectively.
 ω_s : mechanical speed.
 ω : frequency of the sinusoidal waves or electrical speed..
 ϕ_v, ϕ_{vr} : phase of the stator and rotor voltage respect to the rotor position, respectively.
 ϕ_i, ϕ_{ir} : phase of the stator and rotor current respect to the rotor position, respectively.
 $\phi_\lambda, \phi_{\lambda r}$: phase of the stator and rotor flux respect to the rotor position, respectively.
 τ : external torque provided to the machine.
 τ_e : electromechanical torque generated by the machine.
 τ_E : ICE torque.
 θ : rotor position.

Subscripts

abc : phases a,b,c (natural reference frame).
 α, β, γ : direct, quadrature and homopolar axes in the stationary reference frame.
 $d, q, 0$: direct, quadrature and homopolar axes in the arbitrary reference frame.
 D : DFIM.
 s, r, F : stator, rotor and field, respectively.
 W : WRSM

Mathematical Symbols

$\frac{d}{dt}$: differential operator.
 ∂ : gradient of a function.
 \Re : Real Part.

Chapter 1

Introduction

Resume This Chapter briefly describes the motivation of the Thesis based on the evolution of hybrid vehicles since the beginning until now. The chapter ends with the Thesis objectives and the outline of the Thesis.

1.1 Motivation

The electric vehicle (EV) development began between 1832 and 1839, when Robert Anderson invented the first electric car. Practical and more successful electric road vehicles were invented by both American Thomas Davenport and Scotsmen Robert Davidson around 1842. Both inventors were the first to use non-rechargeable electric cells. The improvement in storage batteries invented in 1865 by Frenchmen Gaston Plante and improved in 1881 by Camille Faure paved the way for development of EV [1].

The attention in these vehicles began in the United States in 1891 when Riker built an electric tricycle, and simultaneously Morrison built a six-passenger wagon. Shortly thereafter, in 1897, in New York, began the first commercial application of electric vehicles by a taxi company [1].

The first hybrid electric vehicle (HEV) was invented by Woods in 1916. The label

“hybrid” comes from the internal combustion engine (ICE) and the electric motor Woods vehicle had. [1].

The EV, had many advantages over its 1900's competitors. At that time “the EV did not have the vibration, smell, and noise associated with gasoline cars. Changing gears on gasoline cars was the most difficult part of driving, while electric vehicles did not require gear changes. While steam-powered cars also had no gear shifting, they suffered from long start-up times of up to 45 minutes on cold mornings. The steam cars had less range before needing water than an electric's range on a single charge. The only good roads of the period were in town, causing most travel to be local commuting, a perfect situation for electric vehicles, since their range was limited. The electric vehicle was the preferred choice of many because it did not require the manual effort to start, as with the hand crank on gasoline vehicles, and there was no wrestling with a gear shifter” [1].

The development of EV declined in 1920; United States had a better road system, bringing the need for longer range vehicles. Henry Ford initiated a mass production of internal combustion engine vehicles, which made these vehicles available and affordable. The invention of the electric starter by Kettering in 1912 eliminated the need for the hand crank.

The period compress between 1935 and 1960 was bad years for the development of EV. However, at the sixties a new interest based on the need for alternative vehicles to reduce exhausted emissions of ICE as well as oil dependence began. Since then, there have been a lot of attempts to build a practical EV. Additionally, several legislative and regulatory actions around the world have renewed electric vehicle development efforts.

In the nowadays automotive world, the electric traction is getting back to take the importance used in HEV, combining the advantages of combustion engine (especially its autonomy), those of the electric motor (mainly the possibility of using regenerative braking). Therefore, the use of HEV gives the option to maintain the momentum of the market in the use of fossil fuels, while improving performance with respect to traditional internal combustion vehicles.

Due to the high interest in the HEV, several companies have entered in this business using series and parallel configurations. The vehicles which are currently on the market include: Honda (Civic Hybrid and Insight), Lexus RX 400h, Toyota Prius, GM Hx, Audi (Q7 hybrid and Duo), BMW Concept X3 Efficient Dynamics, Mercedes (BlueTec Hybrid S-Class, Direct Hybrid S-Class and F 600 Hygenius), Mercury Mariner Hybrid, Chevrolet Tahoe Hybrid, Peugeot (307 CC Hybride and 405), Citroen C4 Hybrid, Saab BioPower

Concept Hybrid, Nissan Altima Hybrid, Opel Corsa Hybrid concept, Volkswagen Golf, LA 301, IAD, Iveco Bus, Conceptor, Magnetmotor [35], [13], [15].

1.2 Thesis Objectives

- *General Objective*

To propose, model and simulate a propulsion system for a series hybrid electric vehicle.

- *Specific Objectives*

- To propose a series hybrid electric vehicle propulsion system.
- To model the system using dynamic analysis of electrical machines.
- To model the system using Bond-Graph techniques.
- To evaluate the proposed system using a steady state power analysis.
- To analyze the capacity of the new system for regenerative braking.

1.3 Main contributions of the Thesis

The main contributions of the Thesis are:

- A novel proposal for a series hybrid electric vehicle propulsion system.
- The Bond Graph model of the wound rotor synchronous machine, and its interconnection with a doubly-fed induction machine.
- The Port Controlled Hamiltonian model of the whole system.
- The power analysis for the system.

The principal results of the Thesis were presented in [27].

1.4 Thesis organization

In Chapter 2 the standard configurations for the hybrid electric vehicle are presented as well as some variations on series one, based on this a novel configuration which is composed by a synchronous machine and an induction machine is presented.

The full system dynamics is modelled in Chapter 3. It contains the equations of the three-phase synchronous and induction machines and the transformation that reduces them into dq -models.

In Chapter 4 the Bond Graph model of the DFIM, the WRSM and the whole system is obtained. Then, the Port-Controlled Hamiltonian models of each machine and the whole system are presented. Finally, simulation results of the whole system are depicted.

System balance energy, in particular the possibility of regenerative braking is analyzed in Chapter 5.

Chapter 2

Hybrid Electric Vehicles

Resume

In this Chapter standard hybrid electric vehicle configurations are presented emphasizing series designs. Based on these, a novel configuration is considered. It consists of a synchronous and an induction machine.

2.1 HEV Configurations

Hybrid electrical vehicles (HEV) are the focus of many research interests because they provide good performance and long operating time [16]. Basically, the HEV is composed of an internal combustion engine, an electrical machine and a battery pack.

In this work we focus on the advanced topologies of series HEV. The use of wound-rotor machines (as doubly-fed induction machines) was studied in [9] and [28]. These systems had some performance limitations because they are unable to control intermediate variables between both machines. More control inputs are necessary in order to achieve a good control for HEV purposes. The propulsion system we present consists of a wound-rotor synchronous generator (WRSM) and a doubly-fed induction machine (DFIM). The main advantage of this system is the ability to manage the energy without

a power converter between both machines. In this case the power management is done through the rotor voltages of the DFIM and the field voltage of the WRSM.

The main goal of the HEV is to reduce the CO_2 emissions by means of the regenerative braking, using the electrical machine both as a motor drive or as a generator, which charges or discharges the batteries. It is also desired to keep the drivability performance of the vehicle [26]. Then, the key goals for HEV's are [13]:

- Maximize fuel economy.
- Minimize exhaust emissions (CO_2).
- Guarantee good driving performance.

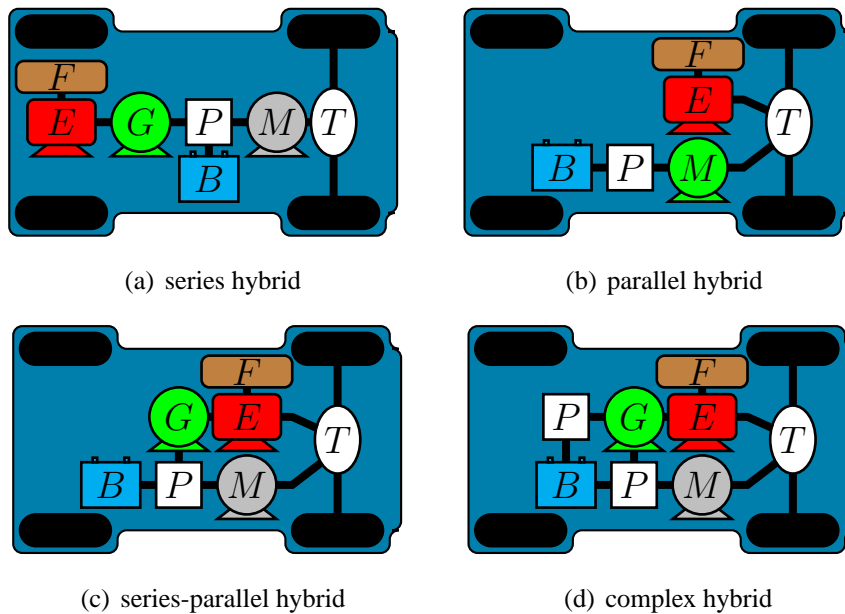


Figure 2.1: HEV topologies.

Figure 2.1 shows some HEV topologies. B represents the battery, E the internal combustion engine (ICE), F the fuel tank, G the electrical generator, M the electrical motor, P the power converter and T the vehicle transmission.

Depending on the interconnection between the different parts of the HEV, this classification can be summarized as:

- **Series Hybrid Electric Vehicle (SHEV):** In a SHEV the ICE mechanical output drives an electric machine, which generates electrical energy. This energy supplies another electric machine, which acts as a motor coupled to the transmission line [13]. The main advantages of this configuration are: on the one hand, the ICE can work at an optimal configuration point finding a compromise between fuel economy and exhaust emissions reduction and, on the other hand, the gear shifting is not necessary. The SHEV is suitable for city cars [17][2][19].
- **Parallel Hybrid Electric Vehicle (PHEV):** The mechanical power is provided simultaneously by the ICE and the electric motor. In this way the ICE can be used for driving while the electric motor for acceleration [13]. There are less energy conversion stages compared to the SHEV, and therefore, the system is more efficient than SHEV, which is the main advantage[17].
- **Series-Parallel Hybrid Electric Vehicle (SPHEV) and Complex Hybrid Electric Vehicle (CHEV):** These configurations combine the features and advantages of a SHEV and a PHEV. The main problem of them is that they are very complex and expensive. The CHEV has bidirectional power flow of the electric motor, that can allow three propulsion power, in this way it is used for dual-axle propulsion [13][17].

2.2 Alternative SHEV's configurations

At the previous Section four generic configurations of HEV's were presented. In this Section we are going to talk about an especial case of SHEV where the stators of the electrical generator and the electrical motor are directly connected. With this, we have found in literature the following schemes: Joint System (JS) and Variable Voltage Variable Frequency (VVVF).

- **Joint System:**

The Joint System, see Figure 2.2, was introduced by Caratuzzolo et al. in [9]. The main feature is the use of a doubly-fed induction machine (DFIM). Then the JS is composed by a DFIM and a squirrel cage induction machine (IM). The induction motor is fed by the DFIM, that has like primary motor an internal combustion engine; the vehicle output torque is provided by the IM.

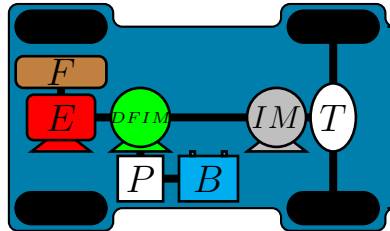


Figure 2.2: The joint system scheme

In this case the DFIM manages all the power flowing through the system (ICE, IM, battery). This power flow is controlled by the rotor voltages of the DFIM using a bidirectional inverter, which connects the DFIM to the battery pack.

The JS has only two degrees of freedom (DFIM rotor voltages), therefore it could not control efficiently the power flux between machine stators and the output torque at the same time.

Some works in control and energy management analysis of the system were presented in [10], [8], [11], [12] and [6].

- **VVVF system:**

A Variable Voltage Variable Frequency scheme (Figure 2.3), was introduced by Ortmeier in [29], [30], [31], it was previously minded to marine applications, but can be used as a particular SHEV. The VVVF use a permanent magnet synchronous machine (PMSM) as a generator, while the mechanical torque is produced by an IM. The stator frequency of both machines is imposed by the mechanical speed of the ICE. In this configuration, the only control input is the torque produced by the ICE.

This system was improved in [28], where the IM was replaced by a DFIM (Figure 2.4). The DFIM allows to store energy into the batteries. All the system is controlled through the DFIM rotor voltages with a bi-directional inverter.

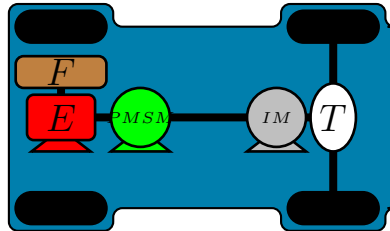


Figure 2.3: VVVF scheme

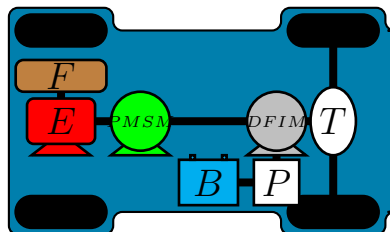


Figure 2.4: VVVF modified scheme

2.3 Direct Synchronous-Asynchronous Conversion System

It is well known that a permanent magnet synchronous machine (PMSM) is more efficient than a wound rotor synchronous machine (WRSM) [34], but the second one has the ability to control the stator voltage through the rotor voltages. In this work a new SHEV scheme is proposed, where the generator is a WRSM which fixes the stator voltage amplitude to a DFIM that acts as motor. This system is called DiSAC (Direct Synchronous-Asynchronous Conversion). An electrical scheme of the DiSAC system is shown in Figure 2.5.

This scheme has four available control inputs:

- DFIM rotor voltages, v_{rd}, v_{rq} .
- WRSM field voltage, v_F .
- ICE torque, τ_E .

To control the system efficiently we must fulfill four specifications namely:

Chapter 3

DiSAC System Model

Resume The full system dynamics is modelled in this Chapter. It describes the dynamics of the three-phase synchronous and induction machines and the transformation that reduces them into dq -model. Finally, the rules that describes the interconnection are also described.

3.1 Three-phase dynamical model

The electrical machines modeling has been widely studied. In general, the dynamic equations that govern the electrical machine behavior are given by two differential equations, one electrical and one mechanical. The first one is given by [25],

$$v(t) = Ri(t) + \dot{\lambda}(t), \quad (3.1)$$

where $v(t)$, $i(t)$ and $\lambda(t)$ are the voltages, currents and fluxes; R is the machine dissipative matrix. Neglecting saturation effects, the fluxes, λ , are related with the currents, i , through the inductances matrix, $\mathcal{L}(\theta)$,

$$\lambda = \mathcal{L}(\theta)i, \quad (3.2)$$

where θ is the rotor position. The inductance matrix shape depends on the machine physical structure. The mechanical equation is described by the Newton's second law,

$$J \frac{d\omega_r}{dt} = -B\omega_r + \tau_e + \tau, \quad (3.3)$$

where J is the inertia, B is the damping coefficient, τ is the external torque provided to the machine and τ_e is the electromechanical torque generated by the machine, which can be written as,

$$\tau_e = \frac{1}{2} i^T \frac{\partial \mathcal{L}(\theta)}{\partial \theta} i. \quad (3.4)$$

As usual, studying electrical machines the following assumptions are considered:

- Symmetrical phases with uniform air-gap and sinusoidally distributed phase windings.
- Infinite permeability of the fully laminated cores.
- Saturation iron losses, end winding and slot effects are neglected.
- Only linear magnetic materials are considered.
- All parameters are constant.

3.1.1 Wound rotor synchronous machine

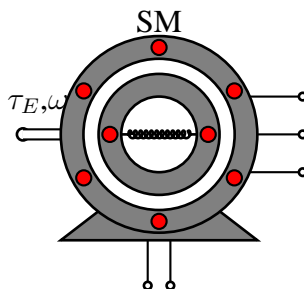


Figure 3.1: Three-phase synchronous machine scheme

A three-phase wound rotor synchronous machine is composed by a three-phase stator winding and a field winding feed with DC voltage at rotor side (Figure 3.1). In synchronous machines, the stator frequency is directly given by the mechanical speed, ω_s

($\omega_s = n_p \omega$, where ω is the electrical speed, n_p is the number of pole pairs). At the stator side, the voltages, currents and fluxes are three-phase variables, while rotor variables, indicated with the F subindex, are one dimensional [25].

$$\begin{aligned} v(t)^T &= [v_{sa}, v_{sb}, v_{sc}, v_F] = [v_s^T, v_F] \in \mathbb{R}^4, \\ i(t)^T &= [i_{sa}, i_{sb}, i_{sc}, i_F] = [i_s^T, i_F] \in \mathbb{R}^4, \\ \lambda(t)^T &= [\lambda_{sa}, \lambda_{sb}, \lambda_{sc}, \lambda_F] = [\lambda_s^T, \lambda_F] \in \mathbb{R}^4. \end{aligned}$$

The three-phase variables are usually considered balanced, i.e.,

$$\begin{aligned} v_s(t)^T &= [v_{sa}, v_{sb}, v_{sc}] = \mathcal{V}_s \left[\cos(\theta + \phi_v), \cos\left(\theta + \phi_v - \frac{2\pi}{3}\right), \cos\left(\theta + \phi_v + \frac{2\pi}{3}\right) \right], \\ i_s(t)^T &= [i_{sa}, i_{sb}, i_{sc}] = \mathcal{I}_s \left[\cos(\theta + \phi_i), \cos\left(\theta + \phi_i - \frac{2\pi}{3}\right), \cos\left(\theta + \phi_i + \frac{2\pi}{3}\right) \right], \\ \lambda_s(t)^T &= [\lambda_{sa}, \lambda_{sb}, \lambda_{sc}] = \mathbf{\Lambda}_s \left[\cos(\theta + \phi_\lambda), \cos\left(\theta + \phi_\lambda - \frac{2\pi}{3}\right), \cos\left(\theta + \phi_\lambda + \frac{2\pi}{3}\right) \right], \end{aligned}$$

where \mathcal{V}_s , \mathcal{I}_s and $\mathbf{\Lambda}_s$ are the amplitudes of the stator voltages, currents and fluxes, respectively, and ϕ_v , ϕ_i and ϕ_λ are their phase respect to the rotor position. The electric dissipation is represented by

$$R = \begin{bmatrix} R_{sW} & 0 & 0 & 0 \\ 0 & R_{sW} & 0 & 0 \\ 0 & 0 & R_{sW} & 0 \\ 0 & 0 & 0 & R_F \end{bmatrix},$$

where R_{sW} and R_F are the stator and field resistances, respectively.

The inductance matrix, $\mathcal{L}(\theta)$, is defined as,

$$\mathcal{L} = \begin{bmatrix} \mathcal{L}_{sW} & \mathcal{L}_{lsW} & \mathcal{L}_{lsW} & \mathcal{L}_m \cos \theta \\ \mathcal{L}_{lsW} & \mathcal{L}_{sW} & \mathcal{L}_{lsW} & \mathcal{L}_m \cos\left(\theta - \frac{2\pi}{3}\right) \\ \mathcal{L}_{lsW} & \mathcal{L}_{lsW} & \mathcal{L}_{sW} & \mathcal{L}_m \cos\left(\theta + \frac{2\pi}{3}\right) \\ \mathcal{L}_m \cos \theta & \mathcal{L}_m \cos\left(\theta - \frac{2\pi}{3}\right) & \mathcal{L}_m \cos\left(\theta + \frac{2\pi}{3}\right) & L_F \end{bmatrix},$$

where \mathcal{L}_{sW} , \mathcal{L}_m and L_F are the stator, magnetization and field inductances, respectively.

τ_e is the electrical torque which can be computed from 3.4,

$$\tau_e = -\mathcal{L}_m i_F \left(i_a \sin \theta + i_b \sin\left(\theta - \frac{2\pi}{3}\right) + i_c \sin\left(\theta + \frac{2\pi}{3}\right) \right). \quad (3.5)$$

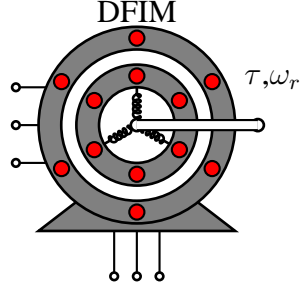


Figure 3.2: Three-phase induction machine scheme.

3.1.2 Doubly-fed induction machine

The DFIM is composed by two three-phase systems, on the stator and on the rotor sides, see Figure 3.2¹. The voltages, currents and fluxes can be written as,

$$\begin{aligned} v(t) &= [v_{sa}, v_{sb}, v_{sc}, v_{ra}, v_{rb}, v_{rc}] = [v_s^T, v_r^T] \in \mathbb{R}^6, \\ i(t) &= [i_{sa}, i_{sb}, i_{sc}, i_{ra}, i_{rb}, i_{rc}] = [i_s^T, i_r^T] \in \mathbb{R}^6, \\ \lambda(t) &= [\lambda_{sa}, \lambda_{sb}, \lambda_{sc}, \lambda_{ra}, \lambda_{rb}, \lambda_{rc}] = [\lambda_s^T, \lambda_r^T] \in \mathbb{R}^6. \end{aligned}$$

The three-phase variables, considering a balanced system, are

$$\begin{aligned} v_s(t)^T &= [v_{sa}, v_{sb}, v_{sc}] = \mathcal{V}_s \left[\cos(\theta + \phi_v), \cos\left(\theta + \phi_v - \frac{2\pi}{3}\right), \cos\left(\theta + \phi_v + \frac{2\pi}{3}\right) \right], \\ v_r(t)^T &= [v_{ra}, v_{rb}, v_{rc}] = \mathcal{V}_r \left[\cos(\theta + \phi_{vr}), \cos\left(\theta + \phi_{vr} - \frac{2\pi}{3}\right), \cos\left(\theta + \phi_{vr} + \frac{2\pi}{3}\right) \right], \\ i_s(t)^T &= [i_{sa}, i_{sb}, i_{sc}] = \mathcal{I}_s \left[\cos(\theta + \phi_i), \cos\left(\theta + \phi_i - \frac{2\pi}{3}\right), \cos\left(\theta + \phi_i + \frac{2\pi}{3}\right) \right], \\ i_r(t)^T &= [i_{ra}, i_{rb}, i_{rc}] = \mathcal{I}_r \left[\cos(\theta + \phi_{ir}), \cos\left(\theta + \phi_{ir} - \frac{2\pi}{3}\right), \cos\left(\theta + \phi_{ir} + \frac{2\pi}{3}\right) \right], \\ \lambda_s(t)^T &= [\lambda_{sa}, \lambda_{sb}, \lambda_{sc}] = \mathbf{\Lambda}_s \left[\cos(\theta + \phi_\lambda), \cos\left(\theta + \phi_\lambda - \frac{2\pi}{3}\right), \cos\left(\theta + \phi_\lambda + \frac{2\pi}{3}\right) \right], \\ \lambda_r(t)^T &= [\lambda_{ra}, \lambda_{rb}, \lambda_{rc}] = \mathbf{\Lambda}_r \left[\cos(\theta + \phi_{\lambda r}), \cos\left(\theta + \phi_{\lambda r} - \frac{2\pi}{3}\right), \cos\left(\theta + \phi_{\lambda r} + \frac{2\pi}{3}\right) \right], \end{aligned}$$

¹The s and r subscripts represent the stator and rotor variables, respectively

where $\mathcal{V}_s, \mathcal{V}_r, \mathcal{I}_s, \mathcal{I}_r, \Lambda_s$ and Λ_r are the amplitudes of the stator and rotor voltages, currents and fluxes, respectively, and $\phi_v, \phi_{vr}, \phi_i, \phi_{ir}, \phi_\lambda$ and $\phi_{\lambda r}$ are their phases respect to the rotor position. The electric dissipation is represented by the following matrix

$$R = \begin{bmatrix} R_{sD} & 0 & 0 & 0 & 0 & 0 \\ 0 & R_{sD} & 0 & 0 & 0 & 0 \\ 0 & 0 & R_{sD} & 0 & 0 & 0 \\ 0 & 0 & 0 & R_r & 0 & 0 \\ 0 & 0 & 0 & 0 & R_r & 0 \\ 0 & 0 & 0 & 0 & 0 & R_r \end{bmatrix},$$

where R_{sD} and R_r are the stator and rotor resistances, respectively.

The inductances matrix, $\mathcal{L}(\theta)$, is defined as,

$$\mathcal{L}(\theta_r) = \begin{bmatrix} \mathcal{L}_{sD} & \mathcal{L}_{sr}(\theta_r) \\ \mathcal{L}_{sr}(\theta_r)^T & \mathcal{L}_r \end{bmatrix} \in \mathbb{R}^{6 \times 6},$$

where the stator, rotor and magnetization inductances sub-matrix are,

$$\mathcal{L}_{sD} = L_{sD} \begin{bmatrix} 1 & \cos(\frac{2\pi}{3}) & \cos(\frac{2\pi}{3}) \\ \cos(\frac{2\pi}{3}) & 1 & \cos(\frac{2\pi}{3}) \\ \cos(\frac{2\pi}{3}) & \cos(\frac{2\pi}{3}) & 1 \end{bmatrix},$$

$$\mathcal{L}_r = L_r \begin{bmatrix} 1 & \cos(\frac{2\pi}{3}) & \cos(\frac{2\pi}{3}) \\ \cos(\frac{2\pi}{3}) & 1 & \cos(\frac{2\pi}{3}) \\ \cos(\frac{2\pi}{3}) & \cos(\frac{2\pi}{3}) & 1 \end{bmatrix},$$

and

$$\mathcal{L}_{sr}(\theta_r) = L_{sr} \begin{bmatrix} \cos(\theta_r) & \cos(\theta_r + \frac{2\pi}{3}) & \cos(\theta_r - \frac{2\pi}{3}) \\ \cos(\theta_r - \frac{2\pi}{3}) & \cos(\theta_r) & \cos(\theta_r + \frac{2\pi}{3}) \\ \cos(\theta_r + \frac{2\pi}{3}) & \cos(\theta_r - \frac{2\pi}{3}) & \cos(\theta_r) \end{bmatrix}.$$

L_{sD} , L_r and L_{sr} are the stator, rotor and magnetization inductances, respectively. It is important to emphasize that the θ_r dependence occurs only in the magnetization inductance sub-matrix.

The electromagnetic torque can be expressed as follows

$$\tau_e = i_s^T \hat{\mathcal{L}}_{sr}(\theta_r) i_r, \quad (3.6)$$

where

$$\hat{\mathcal{L}}_{sr}(\theta_r) = L_{sr} \begin{bmatrix} -\sin(\theta_r) & \cos(\theta_r - \frac{\pi}{6}) & -\cos(\theta_r - \frac{\pi}{6}) \\ -\cos(\theta_r + \frac{\pi}{6}) & -\sin(\theta_r) & \sin(\theta_r + \frac{\pi}{6}) \\ \cos(\theta_r - \frac{\pi}{6}) & \sin(\theta_r - \frac{\pi}{6}) & -\sin(\theta_r) \end{bmatrix}.$$

3.2 The dq -transformation

The dq -transformation allows to simplify the study of power systems [25] [34]. Under the standard assumptions listed previously, this transformation eliminates the θ -depending coefficients of the inductance matrix, reduces a three-phase system into a two-phase system and allows us to describe a tracking problem as a regulation one.

Let us to define a three-phase variables vector as

$$f_{abc}^T = F \left[\cos(\omega t), \cos\left(\omega t - \frac{2\pi}{3}\right), \cos\left(\omega t + \frac{2\pi}{3}\right) \right], \quad (3.7)$$

where F is the amplitude of the sinusoidal waves and ω is its frequency.

The dq -transformation can be split in two parts. Firstly, the three-phase system is reduced to a two-phase system ², $f_{\alpha\beta\gamma} = [f_\alpha, f_\beta, f_\gamma]^T \in \mathbb{R}^3$, through a static reference frame, by means of

$$f_{\alpha\beta\gamma} = T f_{abc} \quad (3.8)$$

and

$$T = \begin{bmatrix} \frac{\sqrt{2}}{\sqrt{3}} & -\frac{1}{\sqrt{6}} & -\frac{1}{\sqrt{6}} \\ 0 & \frac{1}{\sqrt{2}} & -\frac{1}{\sqrt{2}} \\ \frac{1}{\sqrt{3}} & \frac{1}{\sqrt{3}} & \frac{1}{\sqrt{3}} \end{bmatrix}. \quad (3.9)$$

The second part transforms the sinusoidal functions into constants. To this end, a rotating dq -reference K is defined. The new variables $f_{dq} = [f_d, f_q]^T \in \mathbb{R}^2$ are given by

$$f_{dq} = K^{-1} f_{\alpha\beta}, \quad (3.10)$$

where

$$K = e^{J\delta} = \begin{bmatrix} \cos(\delta) & -\sin(\delta) \\ \sin(\delta) & \cos(\delta) \end{bmatrix}, \quad (3.11)$$

δ is an arbitrary function of time and $f_{\alpha\beta}^T = [f_\alpha, f_\beta]$.

The proposed scheme is composed by a DFIM and a SM. In the next sections, the dissipative and inductance matrices of each machine are presented. Then, the $\alpha\beta$ and dq -models are obtained.

²This reduction is due to the balance of the three-phase system and the third component of the resulting vector (so-called homopolar term) is zero.

3.3 The $\alpha\beta$ model

A two-phase model can be obtained using the transformation presented in (3.11). Then equation (3.1) can be rewritten in $\alpha\beta\gamma$ coordinates as

$$v_{\alpha\beta\gamma} = \dot{\lambda}_{\alpha\beta\gamma} + R_{\alpha\beta\gamma} i_{\alpha\beta\gamma}, \quad (3.12)$$

with

$$R_{\alpha\beta\gamma} = TRT^{-1} = R$$

and the fluxes and currents are now related by

$$\lambda_{\alpha\beta\gamma} = L_{\alpha\beta\gamma} i_{\alpha\beta\gamma}, \quad (3.13)$$

where $L_{\alpha\beta\gamma} = T\mathcal{L}T^{-1}$.

Assuming a three-phase equilibrated system ($f_a + f_b + f_c = 0$), the three-phase variables in the $\alpha\beta\gamma$ coordinates yields,

$$\begin{aligned} v_{\alpha\beta\gamma}^T &= [v_\alpha, v_\beta, v_\gamma] = V [\cos(\theta + \phi_v), \sin(\theta + \phi_v), 0], \\ i_{\alpha\beta\gamma}^T &= [i_\alpha, i_\beta, i_\gamma] = I [\cos(\theta + \phi_i), \sin(\theta + \phi_i), 0], \\ \lambda_{\alpha\beta\gamma}^T &= [\lambda_\alpha, \lambda_\beta, \lambda_\gamma] = \Lambda [\cos(\theta + \phi_\lambda), \sin(\theta + \phi_\lambda), 0], \end{aligned}$$

where $V = \frac{\sqrt{3}}{\sqrt{2}}\mathcal{V}$, $I = \frac{\sqrt{3}}{\sqrt{2}}\mathcal{I}$ and $\Lambda = \frac{\sqrt{3}}{\sqrt{2}}\mathbf{\Lambda}$. Note that the third component, γ , is zero and, under the equilibrated three-phase variables assumption, the system dimension is reduced.

Finally, the two-phase system can be rewritten in only the $\alpha\beta$ coordinates as

$$v_{\alpha\beta} = \dot{\lambda}_{\alpha\beta} + R_{\alpha\beta} i_{\alpha\beta} \quad (3.14)$$

with

$$\lambda_{\alpha\beta} = L_{\alpha\beta} i_{\alpha\beta}. \quad (3.15)$$

3.3.1 Wound rotor synchronous machine

For the WRSM, the dissipation and inductance matrices in $\alpha\beta$ -coordinates, are

$$R_{\alpha\beta} = \begin{bmatrix} R_{sW} & 0 & 0 \\ 0 & R_{sW} & 0 \\ 0 & 0 & R_F \end{bmatrix},$$

$$L_{\alpha\beta\gamma} = \begin{bmatrix} L_{sW} & 0 & L_m \cos \theta \\ 0 & L_{sW} & L_m \sin \theta \\ L_m \cos \theta & L_m \sin \theta & L_F \end{bmatrix}.$$

The electrical torque, τ_e , from (3.5) and (3.9)

$$\tau_e = L_m i_F (i_\alpha \sin \theta - i_\beta \cos \theta). \quad (3.16)$$

3.3.2 Doubly-fed induction machine

As for the DFIM, the dissipation and inductance matrices in $\alpha\beta$ -coordinates, are

$$R_{\alpha\beta} = \begin{bmatrix} R_{sD} & 0 & 0 & 0 \\ 0 & R_{sD} & 0 & 0 \\ 0 & 0 & R_r & 0 \\ 0 & 0 & 0 & R_r \end{bmatrix},$$

$$L_{\alpha\beta} = \begin{bmatrix} L_{sD} & 0 & L_{sr} \cos \theta_r & -L_{sr} \sin \theta_r \\ 0 & L_{sD} & L_{sr} \sin \theta_r & L_{sr} \cos \theta_r \\ L_{sr} \cos \theta_r & L_{sr} \sin \theta_r & L_r & 0 \\ -L_{sr} \sin \theta_r & L_{sr} \sin \theta_r & 0 & L_r \end{bmatrix}.$$

The electrical torque, τ_e is derived from (3.6) and (3.9)

$$\tau_e = L_{sr} (i_{s\alpha} i_{r\alpha} \sin \theta_r + i_{s\alpha} i_{r\beta} \cos \theta_r - i_{s\beta} i_{r\alpha} \cos \theta_r + i_{s\beta} i_{r\beta} \sin \theta_r). \quad (3.17)$$

3.4 The dq model

The dq -model is obtained rotating the $\alpha\beta$ reduced model with (3.11). Then, the relationship between fluxes and currents can be rewritten as

$$e^{J\theta} \lambda_{dq} = L_{\alpha\beta} e^{J\theta} i_{dq}$$

or

$$\lambda_{dq} = e^{-J\theta} L_{\alpha\beta} e^{J\theta} i_{dq} = L_{dq} i_{dq}.$$

From the $\alpha\beta$ -electrical model (3.14), with (3.11),

$$\begin{aligned} e^{J\theta} v_{dq} &= R_{\alpha\beta} e^{J\theta} i_{dq} + \frac{d}{dt} (e^{J\theta} \lambda_{dq}) \\ &= R_{\alpha\beta} e^{J\theta} i_{dq} + \frac{d}{dt} (e^{J\theta}) \lambda_{dq} + e^{J\theta} \dot{\lambda}_{dq}. \end{aligned}$$

Then,

$$v_{dq} = e^{-J\theta} R_{\alpha\beta} e^{J\theta} i_{dq} + e^{-J\theta} \frac{d}{dt} (e^{J\theta}) \lambda_{dq} + \dot{\lambda}_{dq}, \quad (3.18)$$

where, using $\frac{d\theta}{dt} = \omega$,

$$e^{-J\theta} \frac{d}{dt} (e^{J\theta}) = e^{-J\theta} \omega \begin{bmatrix} -\sin \theta & -\cos \theta \\ \cos \theta & -\sin \theta \end{bmatrix} = \omega \begin{bmatrix} 0 & -1 \\ 1 & 0 \end{bmatrix} = \omega J_2,$$

and

$$e^{-J\theta} R_{\alpha\beta} e^{J\theta} = R_{\alpha\beta} = R_{dq}.$$

Finally, the dq-model is described by

$$v_{dq} = R_{dq} i_{dq} + J_\omega \lambda_{dq} + \dot{\lambda}_{dq}. \quad (3.19)$$

The mechanical dynamics also follows (3.3), and the electromechanical torque is derived from (3.4), and it depends on the topology of the electrical machine.

Notice that, assuming an equilibrated system, the three-phase variables are, in the dq coordinates

$$\begin{aligned} v_{dq}^T &= [v_d, v_q] = V [\cos \phi_v, \sin \phi_v], \\ i_{dq}^T &= [i_d, i_q] = I [\cos \phi_i, \sin \phi_i], \\ \lambda_{dq}^T &= [\lambda_d, \lambda_q] = \Lambda [\cos \phi_\lambda, \sin \phi_\lambda]. \end{aligned}$$

3.4.1 Wound rotor synchronous machine

As explained above, a generalized dq model of an electrical machine follows equations (3.3) and (3.19). For the WRSM, and after some algebra, the L_{dq} and J_ω matrices are,

$$L_{dq} = \begin{bmatrix} L_s & 0 & L_m \\ 0 & L_s & 0 \\ L_m & 0 & L_F \end{bmatrix},$$

$$J_\omega = \begin{bmatrix} 0 & -\omega_W & 0 \\ \omega_W & 0 & 0 \\ 0 & 0 & 0 \end{bmatrix}.$$

Note that the inductance matrix, L_{dq} does not depend on θ .

The electromechanical torque can be derived from (3.5),

$$\tau_e = -L_m i_F i_q. \quad (3.20)$$

3.4.2 Doubly-fed induction machine

For the DFIM, the generalized dq model of an electrical machine following equations (3.3) and (3.19) can also be applied. After some algebra, the L_{dq} and J_ω matrices are,

$$\mathcal{L}_{dq} = \begin{bmatrix} L_{sD}I_2 & L_{sr}I_2 \\ L_{sr}I_2 & L_rI_2 \end{bmatrix} \in \mathbb{R}^{4 \times 4}, \quad I_2 = \begin{bmatrix} 1 & 0 \\ 0 & 1 \end{bmatrix},$$

$$J_\omega = \begin{bmatrix} \omega_s J_2 & O_{2 \times 2} \\ O_{2 \times 2} & (\omega_s - \omega_D) J_2 \end{bmatrix}, \quad O_2 = \begin{bmatrix} 0 & 0 \\ 0 & 0 \end{bmatrix}.$$

Note that the inductance matrix neither depends on θ .

The generated torque is reduced to,

$$\tau_e = L_m i_{sdq}^T J_2 i_{rdq}. \quad (3.21)$$

3.5 System interconnection

The DiSAC model can be obtained interconnecting the WRSM and the DFIM through the stator side of both machines. The interconnection rules are,

$$v_{sW} = v_{sD}, \quad (3.22)$$

$$i_{sW} = -i_{sD}, \quad (3.23)$$

$$\omega_s = \omega_W. \quad (3.24)$$

Chapter 4

Energy-Based Models

Resume

In this Chapter, energy-based modelling techniques are applied to the DiSAC propulsion system. Bond Graph and Port-Controlled Hamiltonian approaches are used to describe the WRSM and the DFIM dynamics. Thanks to its ability to obtain complex system from the physical interconnection rules, the DiSAC system is finally presented using both modelling methodologies.

4.1 Bond Graph model

“*Bond-Graph*” (BG) is a graphic language to describe the dynamic behavior of physical systems regardless of the work domain. Therefore, is a powerful tool for analyzing complex dynamical systems [7], [23], [32]. This approach is based on the power flow between the different elements of the system. The choice of bond graph allows to describe the systems keeping the information of energy generation, storage, dissipation, and transfer, which can help to design, in a future, a low-level and supervisory control algorithm [23].

The bond graph description permits the integration of submodels easily and, by means of a simple computer algorithm, the simulation-ready equations of a complex model can

be derived. Thus, the physical concepts are similar in their different domains (Table 4.1).

	Effort	Flow
Mechanical	Force (F)	Speed (V)
Mechanical Rotative	Torque (τ)	Angular speed (ω)
Electrical	Voltage (v)	Current (i)
Hydraulic	Pressure (P)	Flow (Q)

Table 4.1: Equivalences between different domains

In BG (Figure 4.1) the vertexes represent the sub-models that are describing the physical phenomenon, and the axis, called “bonds”, represent the ideal point to point energy connection between the ports of the different sub-models. The bond consists of two signals, or *power variables*, with opposite directions, which are called effort ($e(t)$) and flow ($f(t)$).

The power flow direction in the bond is determined by the arrow, which assign only a sign agreement for further analysis.

The causality determines which power variable is the cause (input into its equivalent in block diagram) and which is the result (output). The causality is represented by a orthogonal line to the power bond in the element where the action is forced. For example, in Figure 4.1 the causality states that the element A fixes the effort in B; and B returns a flow as result.

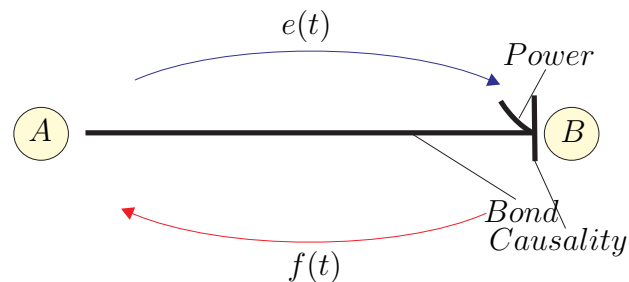


Figure 4.1: Bond Graph

The relationship between flow and effort in a subsystem describes its own behavior. Roughly speaking, the bond graph elements can be classified in: resistors, storage elements, sources, transformers, gyrators and unions.

- **Resistors (R):** These elements dissipate energy. The power flowing through a resistor is always positive and does not assign causality preferred. If the resistance value can be controlled externally is called a modulated resistor (MR). Examples are the frictions, electrical resistors and dampers. The equation that relates the effort and the flow is algebraic and is given by,

$$e = Rf.$$

- **Storage elements (C, I):** Storage elements store all kinds of energy. There are two kinds of storage elements; C-elements and I-elements. Examples are found in capacitors, inductors, masses and springs. In the C-element, the conserved quantity, q (which is a state variable called generalized displacement), results from the net flow accumulation, f , therefore the causality is flow preferred. The differential equation that represents the C-element is,

$$e = \frac{1}{C}q$$

$$q = \int f dt + q(0).$$

For an I-element, the conserved quantity, p (called momentum), results from the net effort accumulation, therefore the causality is effort assigned. The element constitutive equation is,

$$f = \frac{1}{L}p$$

$$p = \int e dt + p(0).$$

- **Sources (Se, Sf):** Sources represent the system interaction with the environment. Examples are voltage sources, current sources (for electrical systems) and external forces and torques (for the mechanical systems). Source elements can impose effort or flow, and, consequently they have the causality allocated depending on the nature of the source.

$$e = e_b$$

$$f = f_b.$$

- **Transformers (TF) and Gytrators (GY):** Transformers and Gytrators are neither storing nor dissipating power and therefore preserving power elements. An ideal energy transformer traduces the effort to effort and the flow to flow, through a transformation relationship n . If n is not a constant, the transformer is a modulated transformer (MTF).

$$\begin{aligned} e_1 &= ne_2 \\ f_2 &= nf_1. \end{aligned}$$

An ideal gyrator represents a domain transformation with gyrator ratio r . If r is not a constant, the gyrator is a modulated gyrator (MGY). Examples are electric motors, pumps and turbines. In the gyrator the effort becomes flow and viceversa.

$$\begin{aligned} e_1 &= rf_2 \\ e_2 &= rf_1. \end{aligned}$$

- **Unions (1,0):** These elements join two or more elements preserving power, it can done keeping the effort or the flow. They are represented by 0 and 1 respectively, i.e., a 0 union represents a node in which all connected efforts each other, and the addition of the connected flows is equal to zero. The 1 union is the dual of the 0 union and represent a node in which all flows that are connected are equal and the efforts addition is equal to zero. In electrical terms, unions 0 and 1 are equivalent to the voltage and current Kirchhoff laws.

Many electrical machines are described using the bond graph approach. From the DC machine [23] or a simple AC generator [5], to three-phase induction machines [4][24]. HEV are also modeled using this graphical tool. In [22], a complete bond graph model for a long urban transit bus is obtained and simulated. A bond graph model of a parallel HEV system is presented in [18], where the electrical machine and internal combustion engine were modeled as an ideal torque source (**Se**-element), while the main contribution was focused in the transmission, aerodynamics and wheel models.

The bond graph models of the electrical machines are obtained from the dynamical equations presented in the previous Chapter. Figures 4.2 and 4.3 represent the developed models for the DFIM and the WRSM, respectively. For this modeling the l-elements L_{lsD} , L_{lr} , L_{lsW} , L_{lF} are defined as

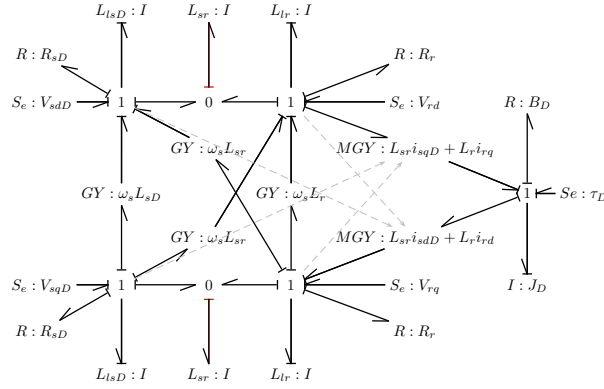


Figure 4.2: Bond Graph model of a doubly-fed induction machine.

$$\begin{aligned}
 L_{lsD} &= L_{sD} - L_{sr}, \\
 L_{lr} &= L_r - L_{sr}, \\
 L_{lsW} &= L_{sW} - L_m, \\
 L_{lF} &= L_F - L_m.
 \end{aligned}$$

Notice that, from the WRSM model, the Bond Graph of a permanent magnet synchronous machine (PMSM) can be easily obtained by replacing the field dynamics by a constant flux, ϕ . It implies to eliminate all elements around the up-right 1-junction, and then the MGY becomes a standard GY-element, with a ϕ -depending gyrator modulus.

The DiSAC system model can be obtained interconnecting the WRSM and the DFIM through the stator side of both machines. The interconnection rules are described in the previous Chapter, equations (3.22), (3.23) and (3.24).

Finally, the Bond Graph scheme for the DiSAC system is shown in Figure 4.4. Notice that, besides the differential causality assignments internal to the two machines, there are extra ones (one for each dq coordinate) due to the way the machines are connected (see the L_{lsD} elements).

In order to obtain a three-phase system description, the dq transformation can be also represented under the BG formalism. Figures 4.5 and 4.6 show the $\alpha\beta$ to dq, and the abc to $\alpha\beta$ transformations, respectively.

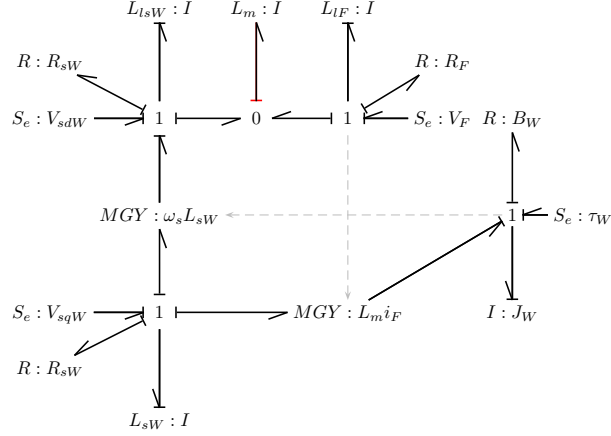


Figure 4.3: Bond Graph model of a wound-rotor synchronous machine.

4.2 Port controlled Hamiltonian model

Port-Controlled Hamiltonian Systems (PCHS) theory provides the mathematical foundation of the Bond Graph approach [20]. Hamiltonian modeling uses the state dependent energy functions to characterize the dynamics of the different subsystems, and connect them using a Dirac structure, which embodies the power preserving network of relations established by the corresponding physical laws. The result is a mathematical model with an specific structure, called port-controlled Hamiltonian system (PCHS) [33], which lends itself to a natural, physics-based analysis and control design.

An explicit PCHS has the form [14]

$$\begin{cases} \dot{x} &= (\mathcal{J}(x) - \mathcal{R}(x))\partial H + g(x)u \\ y &= g^T(x)\partial H \end{cases} \quad (4.1)$$

where $x \in \mathbb{R}^n$ are the energy variables (or state vector), $u, y \in \mathbb{R}^m$ are the port variables, and $H(x) : \mathbb{R}^n \rightarrow \mathbb{R}$ is the Hamiltonian function, representing the energy function of the system. The ∂_x (or ∂ , if no confusion arises) operator defines the gradient of a function of x and, in the sequel, we will take it as a column vector. $\mathcal{J}(x) \in \mathbb{R}^{n \times n}$ is the interconnection matrix, which is skew-symmetric ($\mathcal{J}(x) = -\mathcal{J}(x)^T$), representing the internal energy flow in the system, and $\mathcal{R}(x) \in \mathbb{R}^{n \times n}$ is the dissipation matrix, symmetric and, in physical systems, positive semidefinite ($\mathcal{R}(x) = \mathcal{R}(x)^T \geq 0$), which accounts for the internal losses of the system. Finally, $g(x) \in \mathbb{R}^{n \times m}$ is an interconnection matrix describing the port connection of the system to the outside world. It yields the flow of energy

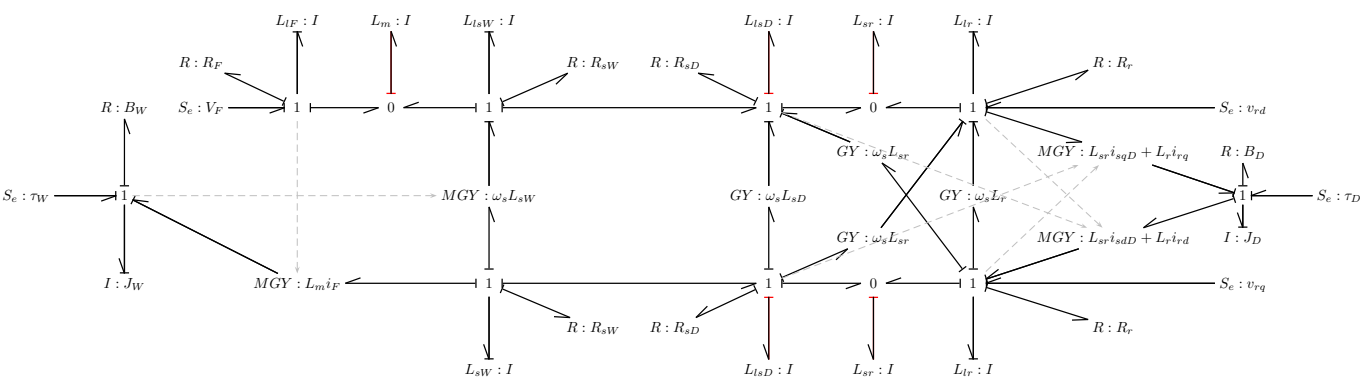
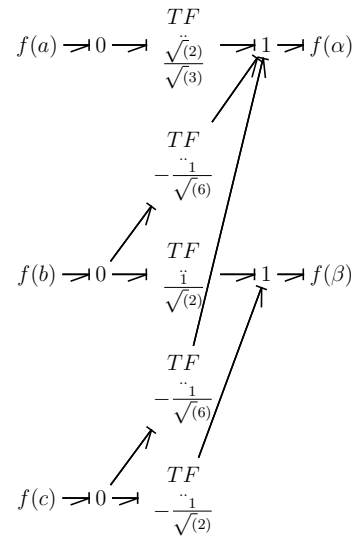
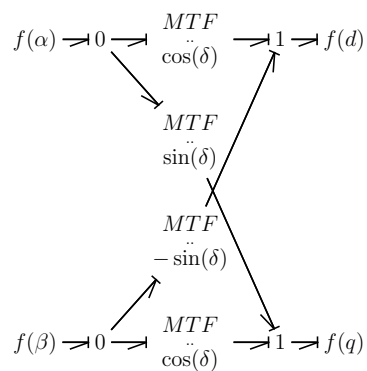


Figure 4.4: Bond Graph model of the DiSAC system.

Figure 4.5: Bond Graph of the T matrix of dq -transformationFigure 4.6: Bond Graph of the K matrix of dq -transformation

to/from the system through the port variables, u and y , which are conjugated, *i.e.* their dot product has units of power.

In this Section, from the standard dq models of the DFIM and WRSM, the PCHS for each machine is derived and the whole interconnected Hamiltonian system is also obtained.

4.2.1 PCHS of a doubly-fed induction machine

The PCHS of a doubly-fed induction machine has been presented in [3]. The Hamiltonian variables are

$$x_D^T = [\lambda_D^T, p_D] = [\lambda_{sD}^T, \lambda_r^T, p_D] \in \mathbb{R}^5,$$

where $\lambda_{sD} = [\lambda_{sDd}, \lambda_{sDq}]^T$ and $\lambda_r = [\lambda_{rd}, \lambda_{rq}]^T$ are the stator and rotor fluxes in dq -coordinates, respectively, $p_D = J_D \omega_D$ is the mechanical momentum, ω_D is the mechanical speed and J_D is the inertia of the rotating parts. Note that the D subindex has been included to refer to the DFIM.

The interconnection and damping matrix are, respectively,

$$\mathcal{J}_D = \begin{bmatrix} -\omega_s L_{sD} J_2 & -\omega_s L_{sr} J_2 & O_{2 \times 1} \\ -\omega_s L_{sr} J_2 & -(\omega_s - \omega_D) L_r J_2 & L_{sr} J_2 i_{sD} \\ O_{1 \times 2} & L_{sr} i_{sD}^T J_2 & 0 \end{bmatrix} \in \mathbb{R}^{5 \times 5},$$

$$\mathcal{R}_D = \begin{bmatrix} R_{sD} I_2 & O_{2 \times 2} & O_{2 \times 1} \\ O_{2 \times 2} & R_r I_2 & O_{2 \times 1} \\ O_{1 \times 2} & O_{1 \times 2} & B_D \end{bmatrix} \in \mathbb{R}^{5 \times 5},$$

where $i_{sD}, i_r \in \mathbb{R}^2$ are the stator and rotor currents, R and L are resistance and inductances¹, ω_s is the stator electric frequency, B_D is the mechanical damping,

$$J_2 = \begin{bmatrix} 0 & -1 \\ 1 & 0 \end{bmatrix}, \quad I_2 = \begin{bmatrix} 1 & 0 \\ 0 & 1 \end{bmatrix}$$

and $O_{* \times *}$ represents zero matrix.

Fluxes, λ_D , and currents, $i_D^T = [i_{sD}^T, i_r^T] \in \mathbb{R}^4$, are related by

$$\lambda_D = \mathcal{L}_D i_D, \tag{4.2}$$

¹Subscripts s and r refers to the stator and rotor, respectively.

where the inductance matrix, \mathcal{L}_D , is

$$\mathcal{L}_D = \begin{bmatrix} L_{sD}I_2 & L_{sr}I_2 \\ L_{sr}I_2 & L_rI_2 \end{bmatrix} \in \mathbb{R}^{4 \times 4}.$$

The port connection is represented by

$$g_D = \begin{bmatrix} I_2 & O_{2 \times 2} & O_{2 \times 1} \\ O_{2 \times 2} & I_2 & O_{2 \times 1} \\ O_{1 \times 2} & O_{1 \times 2} & 1 \end{bmatrix} \in \mathbb{R}^{5 \times 5},$$

with the port variables $u_D^T = [v_{sD}^T, v_r^T, \tau_D]$, where $v_{sD}, v_r \in \mathbb{R}^2$ are the stator and rotor voltages and τ_D is an external torque. The Hamiltonian model is completed with the energy function

$$H_D(x_D) = \frac{1}{2} \lambda_D^T \mathcal{L}_D^{-1} \lambda_D + \frac{1}{2J_D} p_D^2.$$

4.2.2 PCHS of a wound-rotor synchronous machine

A Port-Controlled Hamiltonian model of a synchronous machine, with permanent magnet, can be found in [21]. The wound rotor synchronous machine includes a rotor winding which has to be considered. In this case, the Hamiltonian variables are

$$x_W^T = [\lambda_W^T, p_W] = [\lambda_{sW}^T, \lambda_F, p_W] \in \mathbb{R}^4,$$

where $\lambda_{sW} = [\lambda_{sWd}, \lambda_{sWq}]^T$ is the stator inductor flux in dq -coordinates, λ_F is the rotor (or field) inductor flux, $p_W = J_W \omega_W$ is the mechanical momentum, ω_W is the mechanical speed, and J_W is the inertia of the rotating parts. The W subindex has been included to refer to the WRSM.

The interconnection and damping matrix are, respectively,

$$\mathcal{J}_W = \begin{bmatrix} -\omega_W L_{sW} J_2 & O_{2 \times 1} & -M i_F \\ O_{1 \times 2} & 0 & 0 \\ M^T i_F & 0 & 0 \end{bmatrix} \in \mathbb{R}^{4 \times 4},$$

$$\mathcal{R}_W = \begin{bmatrix} R_{sW} I_2 & O_{2 \times 1} & O_{2 \times 1} \\ O_{1 \times 2} & R_F & 0 \\ O_{1 \times 2} & 0 & B_W \end{bmatrix} \in \mathbb{R}^{4 \times 4},$$

where $i_{sW} \in \mathbb{R}^2$ are the stator currents, i_F is the rotor (or field) current, R and L are resistance and inductances², B_W is the mechanical damping and

$$M = \begin{bmatrix} 0 \\ L_m \end{bmatrix} \in \mathbb{R}^{2 \times 1},$$

with L_m being the mutual inductance.

The WRSM fluxes, λ_W , and currents, $i_W^T = [i_{sW}^T, i_F] \in \mathbb{R}^3$, are related by

$$\lambda_W = \mathcal{L}_W i_W \quad (4.3)$$

and the inductance matrix, \mathcal{L}_W , is

$$\mathcal{L}_W = \begin{bmatrix} L_{sW} I_2 & M \\ M^T & L_F \end{bmatrix} \in \mathbb{R}^{3 \times 3}.$$

The port connection, g_W , is represented by an identity 4×4 matrix,

$$g_W = I_4,$$

with the port variables $u_W^T = [v_{sW}^T, v_F, \tau_W]$, where $v_{sW} \in \mathbb{R}^2$ is the stator voltage, v_F is the rotor (or field) voltage, and τ_W is the applied external torque. Finally, the Hamiltonian function is

$$H_W(x_W) = \frac{1}{2} \lambda_W^T \mathcal{L}_W^{-1} \lambda_W + \frac{1}{2J_W} p_W^2.$$

4.2.3 PCHS of the DiSAC system

As it is shown in Figure 2.5, both machines are interconnected through their stator windings. This implies that

$$v_{sD} = v_{sW} = v_s, \quad (4.4)$$

$$i_{sD} = -i_{sW} = i_s, \quad (4.5)$$

$$\omega_s = \omega_W. \quad (4.6)$$

This particular way of interconnecting the electric machines implies the series connection of two inductors, therefore we define a new variable, $\lambda_s \in \mathbb{R}^2$, such that

$$\lambda_s = \lambda_{sD} - \lambda_{sW}. \quad (4.7)$$

²Subscripts s and F refers to stator and field respectively.

Using (4.2) and (4.3), (4.7) can be written as

$$\lambda_s = (L_{sD} + L_{sW})I_2 i_s + L_{sr}I_2 + M i_F, \quad (4.8)$$

or, differentiating,

$$\dot{\lambda}_s = \dot{\lambda}_{sD} - \dot{\lambda}_{sW}. \quad (4.9)$$

Notice that defining the new state variable as

$$x^T = [\lambda_s^T, \lambda_r^T, \lambda_F, p_D, p_W] \in \mathbb{R}^7$$

and using (4.8) and (4.9), a new Hamiltonian system (4.1) can be obtained. The new Hamiltonian function is

$$H(x) = \frac{1}{2} \lambda^T \mathcal{L}^{-1} \lambda + \frac{1}{2J_D} p_D^2 + \frac{1}{2J_W} p_W^2$$

where fluxes $\lambda^T = [\lambda_s^T, \lambda_r^T, \lambda_F] \in \mathbb{R}^5$ and currents $i^T = [i_s^T, i_r^T, i_F] \in \mathbb{R}^5$ are related by, $\lambda = \mathcal{L}i$. \mathcal{L} is the new inductance matrix

$$\mathcal{L} = \begin{bmatrix} (L_{sD} + L_{sW})I_2 & L_{sr}I_2 & M \\ L_{sr}I_2 & L_r I_2 & O_{2 \times 1} \\ M^T & O_{1 \times 2} & L_F \end{bmatrix}.$$

Finally, the interconnection and dissipation matrices, of the DiSAC system become

$$\mathcal{J} = \begin{bmatrix} -\omega_W(L_{sD} + L_{sW})J_2 & -\omega_W L_{sr}J_2 & O_{2 \times 1} & O_{2 \times 1} & -M i_F \\ -\omega_W L_{sr}J_2 & -(\omega_W - \omega_D)L_r J_2 & O_{2 \times 1} & L_{sr}J_2 i_s & O_{2 \times 1} \\ O_{1 \times 2} & O_{1 \times 2} & 0 & 0 & 0 \\ O_{1 \times 2} & L_{sr} i_s^T J_2 & 0 & 0 & 0 \\ M^T i_F & O_{1 \times 2} & 0 & 0 & 0 \end{bmatrix},$$

$$\mathcal{R} = \begin{bmatrix} (R_{sD} + R_{sW})I_2 & O_{2 \times 2} & O_{2 \times 1} & O_{2 \times 1} & O_{2 \times 1} \\ O_{2 \times 2} & R_r I_2 & O_{2 \times 1} & O_{2 \times 1} & O_{2 \times 1} \\ O_{1 \times 2} & O_{1 \times 2} & R_F & 0 & 0 \\ O_{1 \times 2} & O_{1 \times 2} & 0 & B_D & 0 \\ O_{1 \times 2} & O_{1 \times 2} & 0 & 0 & B_W \end{bmatrix}$$

and

$$g = \begin{bmatrix} O_{2 \times 2} & O_{2 \times 1} & O_{2 \times 1} & O_{2 \times 1} \\ I_2 & O_{2 \times 1} & O_{2 \times 1} & O_{2 \times 1} \\ O_{1 \times 2} & 1 & 0 & 0 \\ O_{1 \times 2} & 0 & 1 & 0 \\ O_{1 \times 2} & 0 & 0 & 1 \end{bmatrix}$$

where the input variables $u^T = [v_r^T, v_F, \tau_D, \tau_W] \in \mathbb{R}^5$.

4.3 Simulation results

In this Section numerical simulations of the DiSAC system are presented in order to validate the obtained models. The WRSM was controlled via a PI controller. The DFIM uses a nested control system. An outer PI controller generates the speed reference for an inner current controller, designed accordingly to [4]. Simulations were performed using the 20sim software which contains a Bond Graph editor.

The DFIM and WRSM parameters are, respectively: $R_{sD} = 0.0823\Omega$, $R_r = 0.0503\Omega$, $L_s = 27.834\text{mH}$, $L_r = 27.834\text{mH}$, $L_{sr} = 27.11\text{mH}$, $B_D = 0.02791\text{Nmrad}^{-1}\text{s}^{-1}$, $J_D = 0.37\text{Kgm}^2$, and $L_{sW} = 26.25\text{mH}$, $R_{sW} = 0.181\Omega$, $L_m = 25.29\text{mH}$, $L_F = 27.19\text{mH}$, $R_F = 0.1002\Omega$ and the WRSM mechanical speed is fixed at $\omega = 314\text{rads}^{-1}$. The machines rated power are: $P_W = 37.5\text{kVA}$ and $P_D = 37\text{kVA}$. The controllers parameters are for the WRSM: $K_p = 30$, $K_i = 3$; for the DFIM inner current loop: $K_p = 0.4$, $K_i = 0.009$, for the outer loop: $K_p = 0.1$, $K_i = 0.01$.

The control objectives are: to regulate the stator voltage ($V = 400\text{V}$), to regulate the DFIM mechanical speed ($\omega_r = 200\text{rads}^{-1}$) and to regulate the stator reactive power ($Q_s = 0\text{VAR}$).

The DFIM load torques starts at $\tau_D = 10\text{Nm}$ and changes to $\tau_D = -10\text{Nm}$ at $t = 2\text{s}$. With these values two modes can be observed. Firstly, the system is storing energy into the batteries. Secondly, power is provided by the batteries.

Figure 4.7 shows the mechanical power flow (computed from $P = \tau\omega$), the rotor active power, P_r , and the stator reactive power³, Q_s . As explained before, the rotor active power is bidirectional and allows to store energy into the batteries.

Figure 4.8 shows the DFIM mechanical speed and its reference. Figure 4.9 shows the rotor amplitude, the stator amplitude and the field voltage, respectively.

³In the dq coordinates, the instantaneous active and reactive power can be computed as $P_r = v_r^T i_r$ and $Q_s = v_s^T J_2 i_s$.

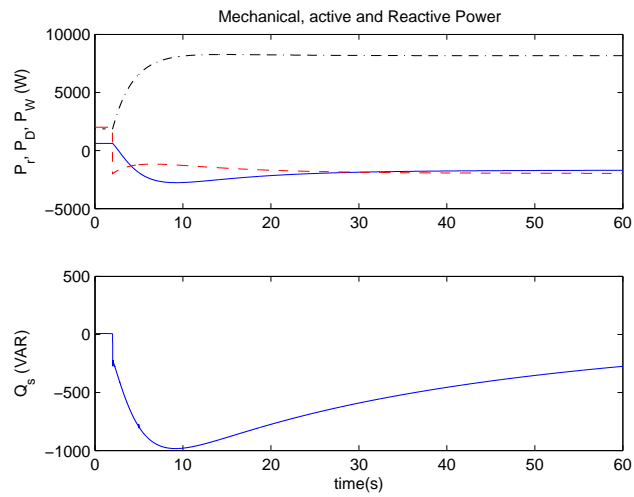


Figure 4.7: Simulation results: WRSM mechanical power (P_W , dashed-dotted black line), DFIM mechanical power (P_D , dashed red line), rotor active power (P_r , continuous blue line), and stator reactive power (Q_s , below).

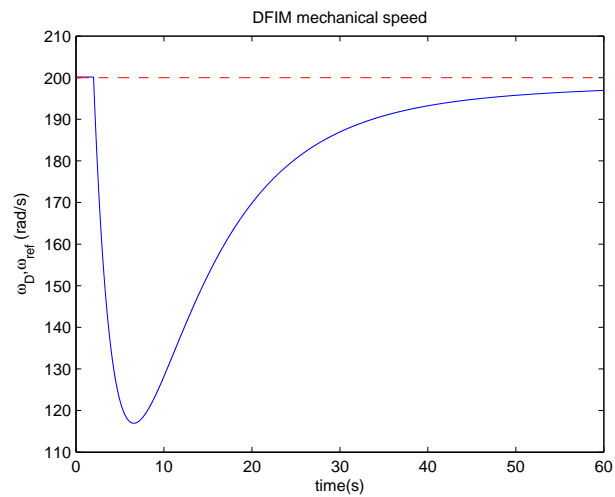


Figure 4.8: DFIM mechanical speed and its reference.

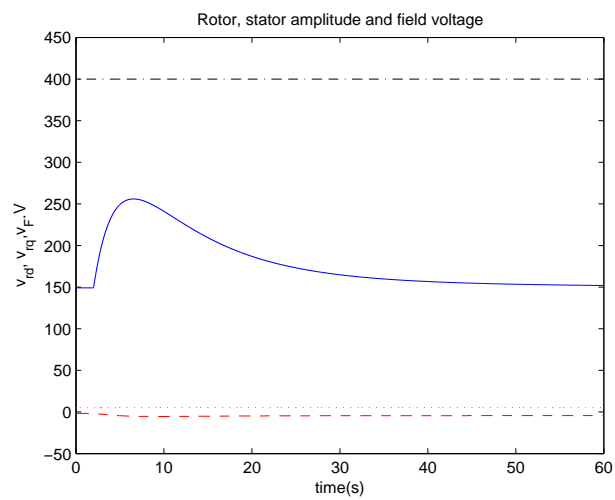


Figure 4.9: Simulation results: Rotor (v_{rd} , continuous blue line, v_{rq} , dashed red line), stator amplitude (V , dashed-dotted black line) and field voltage (v_F , dotted magenta line).

Chapter 5

Power Analysis for the DiSAC System

Resume

This chapter is devoted to the analysis of the system power balance. We wonder to what extent the regenerative braking is worth. We conclude that the system must be modified as a future work in order to be used in a HEV.

5.1 Power analysis of a wound-rotor synchronous machine

In this Section, a steady-state analysis of the energy flowing through a WRSM is done. From the dq -dynamical model, and using the active and reactive power definitions, the energy balance equations are obtained. Finally, approximated expressions for the stator and field power are depicted.

As we have presented in Chapter 3, the WRSM equations in dq -coordinates can be written as,

$$v_{dq} = R_{dq}i_{dq} + J_{\omega}\lambda_{dq} + \dot{\lambda}_{dq}, \quad (5.1)$$

where

$$R_{dq} = \begin{bmatrix} R_{sW} & 0 & 0 \\ 0 & R_{sW} & 0 \\ 0 & 0 & R_F \end{bmatrix},$$

$$L_{dq} = \begin{bmatrix} L_s & 0 & L_m \\ 0 & L_s & 0 \\ L_m & 0 & L_F \end{bmatrix},$$

$$J_\omega = \begin{bmatrix} 0 & -\omega_s & 0 \\ \omega_s & 0 & 0 \\ 0 & 0 & 0 \end{bmatrix}.$$

The mechanical torque is,

$$\tau_e = -L_m i_F i_q. \quad (5.2)$$

From (5.1) the field and stator voltages in steady state are ¹,

$$v_F = R_F i_F$$

and

$$v_s = R_{sW} i_s + \omega_s J_2 L_s i_s + \omega_s L_m \begin{bmatrix} 0 \\ i_F \end{bmatrix}.$$

The active power can be expressed as $P = v^T i$, and taking into account that $J_2^T = -J_2$, the stator voltage transpose vector is,

$$v_s^T = i_s^T R_{sW} - \omega_s L_s i_s^T J_2 + \omega_s L_m \begin{bmatrix} 0 & i_F \end{bmatrix}.$$

Then, the field and stator active power are,

$$P_F = R_F i_F^2, \quad (5.3)$$

$$P_{sW} = i_s^T R_{sW} i_s - \omega_s L_s i_s^T J_2 i_s + \omega_s L_m \begin{bmatrix} 0 & i_F \end{bmatrix} i_s.$$

Finally, using (5.2) and substituting $i^T J_2 i = 0$, the stator active power results in

$$P_{sW} = R_{sW} i_s^2 - \omega_s \tau_e.$$

Neglecting the dissipative losses,

$$P_F \approx 0$$

$$P_{sW} \approx -\omega_s \tau_e.$$

¹For simplicity, the dq subscripts are avoided

5.2 Power analysis of a doubly-fed induction machine

In this Section, an analysis similar to the presented in the previous section is applied to the DFIM. This is also a steady-state analysis of the energy flowing through the DFIM. Expressions for the stator and rotor power of the machine neglecting the dissipative terms are obtained in order to do in the next section a power analysis of the whole system.

As we have presented in Chapter 3, the DFIM equations in dq -coordinates can be written as,

$$v_{dq} = R_{dq}i_{dq} + J_\omega\lambda_{dq} + \dot{\lambda}_{dq}, \quad (5.4)$$

where

$$R_{dq} = \begin{bmatrix} R_{sD} & 0 & 0 & 0 \\ 0 & R_{sD} & 0 & 0 \\ 0 & 0 & R_r & 0 \\ 0 & 0 & 0 & R_r \end{bmatrix},$$

$$\mathcal{L}_{dq} = \begin{bmatrix} L_{sD}I_2 & L_{sr}I_2 \\ L_{sr}I_2 & L_rI_2 \end{bmatrix} \in \mathbb{R}^{4 \times 4}, \quad I_2 = \begin{bmatrix} 1 & 0 \\ 0 & 1 \end{bmatrix},$$

$$J_\omega = \begin{bmatrix} \omega_s J_2 & O_{2 \times 2} \\ O_{2 \times 2} & (\omega_s - \omega_D)J_2 \end{bmatrix}, \quad O_2 = \begin{bmatrix} 0 & 0 \\ 0 & 0 \end{bmatrix}.$$

The electromechanical torque is,

$$\tau_e = L_m i_{sdq}^T J_2 i_{rdq}. \quad (5.5)$$

From (5.4) the stator and rotor voltages in steady state are ²,

$$v_s = R_{sD}i_s + \omega_s J_2 L_{sD}i_s + \omega_s J_2 L_{sr}i_r,$$

and

$$v_r = R_r i_r + (\omega_s - \omega_D)J_2 L_{sr}i_s + (\omega_s - \omega_D)J_2 L_r i_r.$$

The active power can be expressed as $P = v^T i$. The stator and rotor voltages transpose vector are,

$$v_s^T = i_s^T R_{sD} - \omega_s L_{sD} i_s^T J_2 - \omega_s L_{sr} i_r^T J_2$$

and

$$v_r^T = i_r^T R_r - (\omega_s - \omega_D)L_{sr}i_s^T J_2 - (\omega_s - \omega_D)L_r i_r^T J_2.$$

²For simplicity, the dq subscripts are avoided.

Then, the stator and rotor active power results in

$$P_{sD} = i_s^T R_{sD} i_s - \omega_s L_{sD} i_s^T J_2 i_s - \omega_s L_{sr} i_r^T J_2 i_s$$

and

$$P_r = i_r^T R_r i_r - (\omega_s - \omega_D) L_{sr} i_s^T J_2 i_r - (\omega_s - \omega_D) L_r i_r^T J_2 i_r.$$

Using (5.5) and $i^T J_2 i = 0$,

$$P_{sD} = R_{sD} i_s^2 + \omega_s \tau_e, \quad (5.6)$$

and

$$P_r = R_r i_r^2 - (\omega_s - \omega_D) \tau_e. \quad (5.7)$$

Finally, neglecting dissipative losses ($R_{sD} = 0, R_r = 0$), simpler expressions for the stator and rotor active power are obtained. Namely,

$$\begin{aligned} P_{sD} &\approx \omega_s \tau_e \\ P_r &\approx -(\omega_s - \omega_D) \tau_e. \end{aligned}$$

5.3 Power analysis applied to the DiSAC system

In this Section, the steady-state power expressions for the stator and rotor power of both machines are used in order to analyze the power flowing through the DiSAC system. Due the WRSM field power can be neglected and the WRSM stator power is proportional to the ICE applied torque, the HEV power can be analyzed using the DFIM power expressions.

As a result of the DFIM design, the DFIM speed is bounded by zero and two times the stator frequency ($0 < \omega_D < 2\omega_s$). We will analyze the following four cases in order to take an idea of the system behavior, $\omega_D = 0$, $\omega_D = \omega_s$, $\omega_D = 2\omega_s$ and $\omega_D = n\omega_s$.

5.3.1 Vehicle stopped

When the vehicle is stopped the DFIM speed is equal to zero ($\omega_D = 0$), the stator and rotor power are

$$P_{sD} \approx \omega_s \tau_e$$

and

$$P_r \approx -\omega_s \tau_e.$$

The machine is working as a transformer, all the power is flowing from the stator to the rotor or viceversa, depending on the torque sign.

5.3.2 Vehicle running at the synchronous speed

At synchronous speed, $\omega_D = \omega_s$, then, the stator and rotor power are

$$P_{sD} \approx \omega_D \tau_e,$$

and

$$P_r \approx 0.$$

The rotor neither absorbs nor provides power. The stator power is approximately equal to the mechanical power ($P_\omega = \omega_D \tau_e$), then, all the power is flowing from the stator to the mechanical axis or viceversa, depending on the torque sign.

5.3.3 Vehicle running at twice the synchronous speed

This speed means, $\omega_D = 2\omega_s$, then, the stator and rotor power are

$$P_{sD} \approx \omega_s \tau_e = \frac{\omega_D \tau_e}{2},$$

and

$$P_r \approx \omega_s \tau_e = \frac{\omega_D \tau_e}{2}.$$

The stator and the rotor power are equal each other and its addition is the mechanical power. In motor mode ($\tau_e > 0$), the mechanical power comes, in equal parts, from the stator and the rotor. In regenerative braking ($\tau_e < 0$), half of the power is absorbed by the stator and half of the power is absorbed by the rotor.

5.3.4 General analysis

A general analysis is done with $\omega_D = n\omega_s$, $n \in \mathbb{R}$

$$P_{sD} \approx \omega_s \tau_e = \frac{\omega_D \tau_e}{n},$$

and

$$P_r \approx (n-1)\omega_s \tau_e = \frac{(n-1)\omega_D \tau_e}{n}.$$

The stator power plus the rotor power is the mechanical power. In motor mode ($\tau_e > 0$), the mechanical power is provided for the stator and the rotor. In regenerative braking

($\tau_e < 0$), a part of the power is absorbed by the stator and another part of the power is absorbed by the rotor.

Although, the stator is always absorbing or providing power, the unique exception is when $n \gg 1$. This operation point is not desired, because it increments the reactive power losses. Then, in regenerative braking the stator is always absorbing power that can not be controlled with the proposed system. We conclude that the system must be modified in order to control this power.

Chapter 6

Conclusions and future work

A novel series hybrid electric vehicle propulsion system that can be controlled through the rotor voltages of every machine was proposed. This system has the advantage in our knowledge that the rotor converters could be smaller than stator converters in traditional machines. The proposed system defines a novel architecture for the study of isolated generation or a series HEV propulsion system.

This system composed by several subsystems was modeled and simulated in the electrical and mechanical domains. Additionally, two energy-based models were presented following the Hamiltonian formalism and the Bond Graph approach. Simulations results have also been presented. The use of the Bond Graph technique, thanks to easy sub-models integration, allows to complement the presented model with other mechanical (transmission, wheels, aerodynamics...) and electrical parts (power converters, batteries,...).

There is just one operating point where the stator does not absorb power in regenerative braking and, this condition occurs when the ICE is stopped ($\omega_s = 0$). The maximum power that can be absorbed through the rotor when $\omega_s \neq 0$ is the half of the mechanical power in a standard designs. Hence, the proposed configuration must be modified.

As we conclude, the DiSAC system must be modified in order to guarantee a complete controlled regenerative braking. To this end, an inverter could be included between the stator of both machines and the battery pack. This converter would permit to store the energy absorbed by the stator of the DFIM while the regenerative braking occurs and apply extra power to the stator at another operation points. An electrical scheme of the proposed modified DISAC system is shown in figure 6.1.

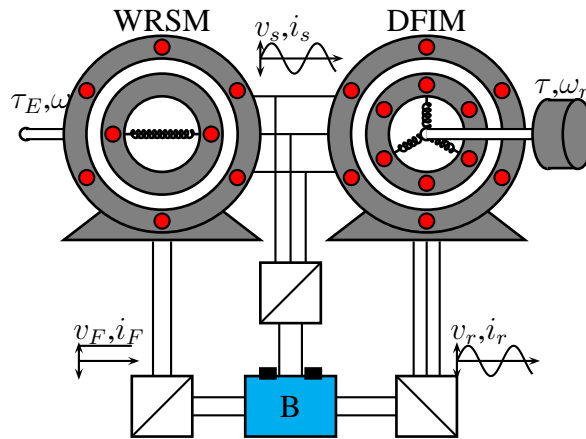


Figure 6.1: Electrical scheme of the modified DiSAC system.

In future works, the modified DiSAC system must be analyzed in order to show its behavior. Then, a robust controller and an energy management for the modified DiSAC system must be designed and implemented at laboratory and at an actual vehicle.

Also, a model of the HEV mechanical parts must be included to complete the system. The complete model behavior with the designed controllers must be simulated using standard profiles for vehicles.

Bibliography

- [1] About. History of electric vehicle, 2002. Available in <http://inventors.about.com/library/weekly/aacarselectrica.htm>. 1, 2
- [2] M. Al-Atabi and T. Yusaf. Experimental investigation of a single cylinder diesel engine as a hybrid power unit for a series hybrid electric vehicle. In *Proc. IEEE Student Conference on Research and Development*, pages 261–264, 2002. 7
- [3] C. Batlle, A. Dòria-Cerezo, and R. Ortega. Power Flow Control of a Doubly-Fed Induction Machine Coupled to a Flywheel. *European Journal of Control*, 11(3):209–221, 2005. 29
- [4] C. Batlle and A. Dòria. Energy-based modeling and simulation of the interconnection of a back-to-back converter and a doubly-fed induction machine. In *American Control Conference*, pages 1851–1856, 2006. 24, 33
- [5] C. Batlle and A. Dòria-Cerezo. Bond graph models of electromechanical systems. the ac generator case. In *IEEE Int. Symp. on Industrial Electronics*, 2008. 24
- [6] M. Becherif, R Ortega., E Mendes., and S. Lee. Passivity-based control of a doubly-fed induction generator interconnected with an induction motor. In *Proc. of the 42nd IEEE Conference on Decision and Control*, pages 5657–5662, 2003. 8
- [7] J. Broenik. Introduction to physical systems modelling with bond graphs. Technical report, University of Twente, 1999. 21
- [8] P. Caratozzolo. *Nonlinear Control Strategies of an Isolated Motion System with a Double-Fed Induction Generator*. PhD thesis, Technical University of Catalonia, 2003. 8
- [9] P. Caratozzolo, E. Fossas, J. Pedra, and J. Riera. Dynamic modeling of an isolated motion system with dfig. In *Proc. of the VII IEEE International Power Electronics Congress*, pages 287–292, 2000. 5, 7

- [10] P. Caratozzolo, E. Fossas, and J. Riera. Nonlinear control of an isolated motion system with dfig. In *Proc. 15th IFAC World Congress*, 2002. 8
- [11] P. Caratozzolo, M. Serra, C. Ocampo, and J. Riera. A proposal for the propulsion system of a series hybrid electric. In *Proc. IEEE 34th Annual Power Electronics Specialist Conference*, pages 586–591, 2003. 8
- [12] P. Caratozzolo, M. Serra, and J. Riera. Energy management strategies for hybrid electric vehicles. In *Proc. IEEE International Electric Machines and Drives Conference*, pages 241–248, 2003. 8
- [13] C. Chan. The state of the art of electric and hybrid electric vehicles. In *Proceedings of the IEEE*, volume 90, 2002. 3, 6, 7
- [14] M. Dalsmo and A. van der Schaft. On representations and integrability of mathematical structures in energy-conserving physical systems. *SIAM J. Control Optim.*, 37:54–91, 1998. 26
- [15] El diferencial. Several articles.
Available in <http://www.eldiferencial.com.mx>. 3
- [16] M. Ehsani, Y. Gao, S.E. Gay, and A. Emadi. *Modern Electric, Hybrid Electric, and Fuel Cell Vehicles: Fundamentals, Theory, and Design*. CRC, Boca Raton, FL, 2004. 5
- [17] A. Emadi, K. Rajashekara, S. Williamson, and S. Lukic. Topological overview of hybrid electric and fuel cell vehicular power system architectures and configurations. *IEEE Transactions on Vehicular Technology*, 54(3):763–770, May 2005. 7
- [18] M. Filippa, C. Mi, J. Shen, and C. Stevenson. Modeling of a hybrid electric vehicle powertrain test cell using bond graphs. *IEEE Transactions on Vehicular Technology*, 54(3):837–845, 2005. 24
- [19] M. Gokasan, S. Bogosyan, and D. Goering. Sliding mode based powertrain control for efficiency improvement in series hybrid-electric vehicles. *IEEE Transactions on Power Electronics*, 21:779–790, May 2006. 7
- [20] G. Golo, A.J. van der Schaft, P.C. Breedveld, and B. Maschke. Hamiltonian formulation of Bond Graphs. In *Workshop NACO II*, pages 2642–2647, 2001. 26
- [21] Y. Guo, Z. Xi, and D. Cheng. Speed regulation of permanent magnet synchronous motor via feedback dissipative hamiltonian realisation. *IET Control Theory Appl.*, 1(1):281–290, 2007. 30

- [22] G. Hubbard and K. Youcef-Toumi. Modeling and simulation of a hybrid-electric vehicle drivetrain. In *Proc. of the 1997 American Control Conference*, volume 1, pages 636–640, 1997. 24
- [23] D. Karnopp, D. Margolis, and R. Rosenberg. *System Dynamics: Modeling and Simulation of Mechatronic Systems*. John Wiley and Sons, Inc, 2006. 21, 24
- [24] J. Kim and M. Bryant. Bond graph model of a squirrel cage induction motor with direct physical correspondence. *Journal of Dynamic Systems, Measurement and Control*, 22:461–469, 2000. 24
- [25] P. Krause, O. Wasynczuk, and S. Sudhoff. *Analysis of Electric Machinery and Drive Systems*. John-Wiley and Sons, 2002. 11, 13, 16
- [26] J.M. Miller. *Propulsion systems for hybrid vehicles*. IEE, Power and Energy series, 2004. 6
- [27] R. S. Muñoz-Aguilar, A. Dòria-Cerezo, and P. F. Puleston. Energy-based modelling and simulation of a series hybrid electric vehicle propulsion system. In *Proc. European Conference on Power Electronics and Applications*, 2009. 3
- [28] T. Ortmeier. Variable voltage variable frequency options for series hybrid vehicles. In *Proc. of IEEE Conference on Vehicle Power and Propulsion*, pages 262–267, 2005. 5, 8
- [29] T. Ortmeier, L. Ban, K. Joshi, and X. Yan. Novel variable voltage variable frequency electric drive. In *Proc. of the Large Engineering Systems Conference on Power Engineering*, pages 44–49, 2003. 8
- [30] T. Ortmeier and X. Yan. Novel electric drive with power regenerating capability: modeling and simulation. In *Proc. of 11th International Conference on Harmonics and Quality of Power*, pages 794–800, 2004. 8
- [31] T. Ortmeier and X. Yan. Pulse load capability for vvvf propulsion drives. In *Proc. of IEEE Electric Ship Technologies Symposium*, pages 340–346, 2005. 8
- [32] A. Samantaray. About bond graphs, 2005.
Available in <http://www.bondgraph.info/about.html>. 21
- [33] A. van der Schaft. *L₂ gain and passivity techniques in nonlinear control*. Springer, 2000. 26
- [34] P. Vas. *Vector Control of AC Machines*. Oxford University Press, 1994. 9, 16
- [35] J. West. Dc, induction, reluctance and pm motors for electric vehicles. *Power Engineering Journal*, pages 77–88, 1994. 3